Robotica (2024), **42**, pp. 3532–3551
doi:10.1017/S0263574724001516

CAMBRIDGE UNIVERSITY PRESS

RESEARCH ARTICLE

An intelligent fixed-time super-twisting sliding mode control of the uncertain hybrid mechanism

Xue Li and Guoqin Gao

School of Electrical and Information Engineering, Jiangsu University, Zhenjiang, Jiangsu Province, China
Corresponding author: Guoqin Gao; Email: gqgao@ujs.edu.cn

Received: 18 December 2023; **Revised:** 3 July 2024; **Accepted:** 9 July 2024; **First published online:** 3 October 2024

Keywords: fixed-time convergence; hybrid mechanism; neural network; super-twisting algorithm; sliding mode control

Abstract

In order to improve the global convergence performance of the super-twisting sliding mode control (STSMC) for the uncertain hybrid mechanism, especially in the high-speed scenario, and enhance the robustness of hybrid mechanism system to the uncertainties with a wide range of changes, an intelligent fixed-time super-twisting sliding mode control (IFTSTSMC) is proposed. Firstly, a fixed-time super-twisting sliding mode control (FTSTSMC) algorithm is designed by adding the exponential power terms with the fixed-time performance parameters in sliding variables and the transcendental function of the super-twisting algorithm in order to enhance the global convergence performance of the STSMC. Secondly, the existence condition of FTSTSMC for the uncertain hybrid mechanism is analyzed. The IFTSTSMC is designed by introducing RBF neural network to break through the limited range of uncertainties in FTSTSMC and enhance the robustness of hybrid mechanism system to the uncertainties with a wide range of changes. Then, the Lyapunov stability of the proposed method and the global fixed-time convergence of the system are proved theoretically. Finally, the effectiveness and superiority of the proposed control method are verified by the simulation and the automobile electro-coating conveying prototype experiment comparing with two classical finite-time sliding mode control methods.

1. Introduction

The hybrid mechanism, which consists of parallel mechanism and series mechanism, has the advantages of high precision, high rigidity, and strong bearing capacity. It has been widely concerned by many research fields such as industrial manufacturing, medical assistance, and so on [1–5]. From the control point of view, the hybrid mechanism can be regarded as a multi-input-output, strongly coupled nonlinear system that is affected by various uncertain factors, such as modeling errors, joint friction, and external disturbance. How to achieve the high performance tracking control of the uncertain hybrid mechanism is still a challenging task [6].

At present, the tracking control methods for the uncertain hybrid mechanism have the fuzzy proportional-integral-derivative (PID) control [7], adaptive dynamic coupling control [8], inverse optimal control [9], sliding mode control (SMC) [10, 11], and so on. Compared with other control methods, SMC has the advantage of insensitivity to the variations of parameters and disturbances; it does not need to establish accurate models and design complex parameters, which has received more attention in the tracking control of the uncertain hybrid mechanism [12, 13]. Based on the relationship between the states of the system and sliding mode variables, SMC can be classified into first-order sliding mode control (FOSMC) [14, 15], second-order sliding mode control (SOSMC) [16–18], and higher-order sliding mode control (HOSMC) [19–22]. Considering from the control of the uncertain hybrid mechanism, FOSMC represents the most fundamental form of SMC. Its theoretical foundation is relatively straightforward and lucid, and it has good extensibility. In addition, the first-order sliding mode controller is designed based on the sliding mode surface which reflects the response change rate of the system, and

the states of the system are evaluated by designing the first-order derivative of this surface. The sliding mode surface generally has a large slope, enabling the sliding mode to rapidly adjust the variables of control and maintain the stability of the system even when the control signals are saturated. However, the derivative of the sliding mode surface function varies constantly as it depends on the current states of the system. The variation of the derivative will cause the sliding mode surface function to be not precisely zero, and it oscillates back and forth on both sides of zero. Therefore, the high-frequency switching of the control can result in the chattering problem [23]. HOSMC adjusts the convergence rate and stability of the system by introducing multiple state variables and control laws, so that the system can reach the desired state [24]. However, compared with FOSMC, the design of HOSMC is more complicated, and more control parameters need to be designed, which increases the difficulty of design and calculation. Accordingly, more tests and adjustments are needed for its control parameters, and the difficulty of control application is increased. As an extension of FOSMC, the SOSMC can extend the relative order while maintaining the excellent performance of FOSMC, and it is simpler than HOSMC. Additionally, the control quantities can be essentially continuous in time, which can effectively reduce the chattering without sacrificing the robustness of the controller. Therefore, this paper intends to improve the SOSMC method to improve the stability and robustness of the uncertain hybrid mechanism system.

The primary kinematic structure of parallel/hybrid robot is the parallel mechanism. At present, SOSMC has been introduced into parallel/hybrid robot [25–28]. For the parallel robot, the second-order integral SMC was combined with the synchronization strategy to reduce the synchronization error of the system and improved the control precision in the environment with external disturbances in [25]. For the hybrid robot, a new compound error was formed by combining the tracking error and synchronization error of the system in [26]. Based on the new compound error, the second-order nonsingular fast terminal SMC was designed. For the uncertain parallel robot, the STSMC was used to solve the trajectory tracking problem of the system in [27, 28]. Among them, the STSMC based on genetic algorithm and global nonlinear sliding surface was proposed in [27]. The method employed a genetic algorithm to minimize the optimal parameters, and SMC had global characteristics, which can eliminate the error or disturbances of the system in the arrival stage. A fast time-varying gain adaptive STSMC was proposed in [28] by matching the sliding mode controller with feedforward action based on dynamic inversion. The proposed method ensured the finite-time convergence, robustness against disturbances, and noise filtering. Among the SOSMC methods mentioned above, the STSMC method does not need the derivative information of the sliding mode surface. Moreover, when the relative order of the system is 1, this algorithm does not need to introduce new control parameters and can still maintain the convergence accuracy and small chattering characteristics of the SOSMC. However, for the STSMC with nonlinear saturation term, considering the existing STSMC based on asymptotic or finite-time stability theory which convergence time is theoretically infinite and related to the initial state information of the system, the convergence rate needs to be improved when it is applied to the uncertain hybrid mechanism, especially the high-speed scenario.

When the system is asymptotic convergence [25, 26], the states of the system theoretically approach the target states at infinity. Especially when the system is in a time-sensitive application scenario, the asymptotic convergence cannot meet the real-time requirements of the system. Therefore, the finite-time control method is proposed [29]. In [30], the finite-time stabilization of the tension leg platforms (TLP) was discussed. Compared with the asymptotic convergence control method, the finite-time control method achieves faster convergence rate near the tunable zero point, but the convergence time obtained by the finite-time control method depends on the initial states of the system, and the initial state information of the actual system is often difficult to obtain accurately. Therefore, the fixed-time stability was first proposed in [31] to solve the problem that the convergence time is related to the initial state information of the system when the system is stable in finite-time. In the researches related to fixed-time control method, the local fixed-time SMC and the FTSTSMC were proposed in [32, 33], respectively. However, the methods mentioned above can only achieve the fixed-time convergence in the reaching phase of SMC without considering the convergence performance in the sliding phase. Therefore, the methods can only achieve the local convergence performance of the system. In order to achieve global

convergence performance of the hybrid mechanism system, this paper intends to introduce the design idea of fixed-time control into the STSMC. By improving sliding variables and the transcendental function of the super-twisting algorithm, the hybrid mechanism system can converge in fixed-time that can be preset, so that the uncertain hybrid mechanism system can obtain global convergence performance.

Through the above design, the FTSTSMC with the improved transcendental function is achieved and improves the convergence performance of the uncertain hybrid mechanism system. However, when the uncertainties of the hybrid mechanism change in a wide range, the existence condition of SMC is destroyed, resulting in the failure of the robustness for FTSTSMC. Therefore, the existence condition of FTSTSMC for the uncertain hybrid mechanism is analyzed. The IFTSTSMC is designed by introducing radial basis function (RBF) neural network to break through the limited range of uncertainties in FTSTSMC and enhance the robustness of hybrid mechanism system to the uncertainties with a wide range of changes.

The contributions of this paper are as follows:

- In order to improve the global convergence performance of the super-twisting sliding mode control (STSMC) for the uncertain hybrid mechanism, especially in the high-speed scenario, the design idea of the fixed-time control is introduced into the STSMC. By adding the exponential power term with the fixed-time performance parameter in sliding variables and the transcendental function of super-twisting algorithm, the convergence performance of STSMC in the reaching stage and sliding stage is improved, so as to achieve the convergence of the uncertain hybrid mechanism system in fixed-time which can be preset. Therefore, the uncertain hybrid mechanism system can obtain better global convergence performance.
- In order to enhance the robustness of hybrid mechanism system to the uncertainties with a wide range of changes, the existence condition of FTSTSMC for the uncertain hybrid mechanism is analyzed, and RBF neural network is further introduced into FTSTSMC. IFTSTSMC is designed to break through the limited range of uncertainties in the FTSTSMC by combining the approximation value related to Gaussian kernel function in the neural network with FTSTSMC. Therefore, the IFTSTSMC designed for the uncertain hybrid mechanisms can enhance the robustness of hybrid mechanism system to the uncertainties with a wide range of changes.

The other parts of this paper are as follows: the second part gives the dynamic model and problem conception of the hybrid mechanism. The IFTSTSMC controller is presented in the third part. In the fourth and fifth parts, the results of simulation and prototype experiments are given respectively. Finally, the conclusion is given. The overview diagram of the paper is shown in Figure 1.

2. Dynamic model and problem formulation

The dynamic model of the hybrid mechanism in joint space can be expressed as

$$M(q)\ddot{q} + C(q,\dot{q})\dot{q} + G(q) = \tau \tag{1}$$

where $q = (q_1, \cdots, q_N)^T$ is the joint posture vector, $\dot{q} = (\dot{q}_1, \cdots, \dot{q}_N)^T$ is the joint velocity vector, $M(q) \in R^{n\times n}$ is the inertia matrix, $C(q,\dot{q})$ is the Gauche and centrifugal force item, $G(q)$ is the gravity term, and τ is the joint driving force/torque.

Taking into account the effects of modeling errors, joint friction, external disturbances, and load variation during actual operation, the dynamic model (1) can be described as

$$[\hat{M}(q) + \Delta M(q)]\ddot{q} + [\hat{C}(q,\dot{q}) + \Delta C(q,\dot{q})]\dot{q} + [\hat{G}(q) + \Delta G(q)] + N(t) = \tau + d \tag{2}$$

where $\Delta M(q)$, $\Delta C(q,\dot{q})$, $\Delta G(q)$ denote the uncertain terms in $M(q)$, $C(q,\dot{q})$, $G(q)$, respectively. $M(q) = \hat{M}(q) + \Delta M(q)$, $C(q,\dot{q}) = \hat{C}(q,\dot{q}) + \Delta C(q,\dot{q})$, $G(q) = \hat{G}(q) + \Delta G(q)$, $N(t)$ are the frictional force and d is the external random disturbances.

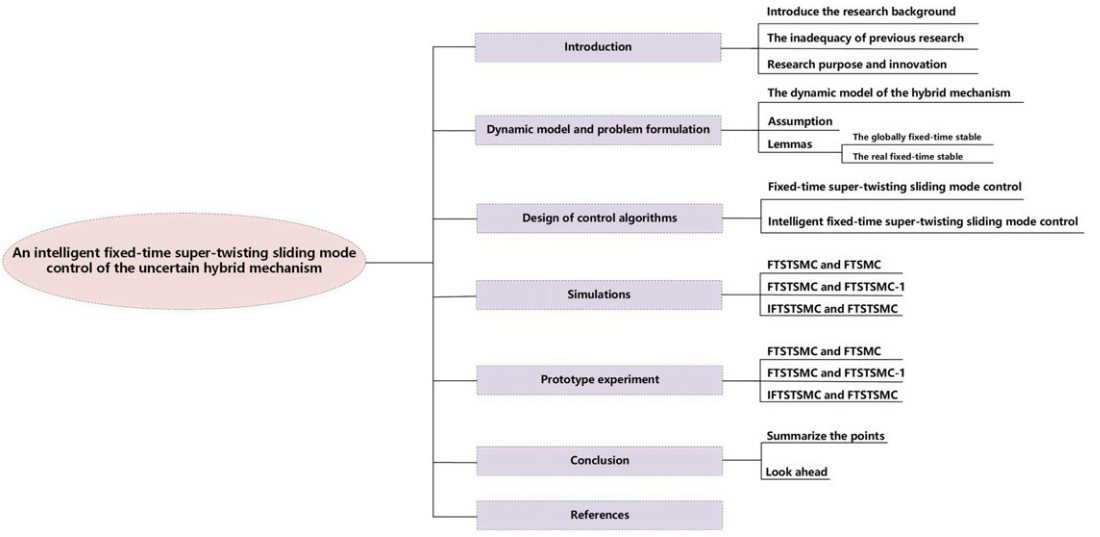

Figure 1. *The overview diagram of the paper.*

Further, the dynamic model (2) of the hybrid mechanism can be rewritten as

$$\ddot{q} = \hat{M}^{-1}[\tau - \hat{C}(q,\dot{q})\dot{q} - \hat{G}(q)] + D(t) \tag{3}$$

where $D(t) = \hat{M}^{-1}[d - \Delta M(q)\ddot{q} - \Delta C(q,\dot{q})\dot{q} - \Delta G(q) - N(t)]$ denotes the set total disturbances term containing modeling errors, joint friction, external disturbances, and load variation.

Let

$$\begin{aligned} x_1 &= q \\ x_2 &= \dot{x_1} = \dot{q} \end{aligned} \tag{4}$$

then

$$\begin{aligned} \dot{x}_1 &= x_2 \\ \dot{x}_2 &= f(x) + g(x)u + D(x) \end{aligned} \tag{5}$$

where $f(x) = -\hat{M}^{-1}[\hat{C}(q,\dot{q})\dot{q} + \hat{G}(q)]$, $g(x) = \hat{M}^{-1}$, $u = \tau$.

Let the desired trajectory of the joints be x_{1d}, in order to realize that the actual trajectory x_1 can be tracked to the desired trajectory x_{1d} in fixed-time, that is, the tracking error $e = x_1 - x_{1d}$ converges to 0 in fixed-time; the following assumptions and lemmas are given.

Assumption 1. $\|D(x)\| \leq \delta$, where $\delta > 0$.

Lemma 1. [34] *Consider the system*

$$\dot{x}(t) = f(t,x), \quad x(t_0) = x(t_0) \tag{6}$$

where $x(t) \in R^n$ is the state variable of the system, $f(t,x)$ denotes a smooth nonlinear function, and the origin is assumed to be the equilibrium point of the system. If there is a continuous radial bounded function $V{:}R^n \to R_+ \cup \{0\}$ satisfying

$$V(x) \leq -\varphi_1 V^P(x) - \varphi_2 V^Q(x)$$

where $\varphi_1, \varphi_2 > 0$, $P > 1$, $0 < Q < 1$, then the system (6) is said to be globally fixed-time stable, and its convergence time T satisfies

$$T \leq T_{max} := \frac{1}{\varphi_1(P-1)} + \frac{1}{\varphi_2(1-Q)}$$

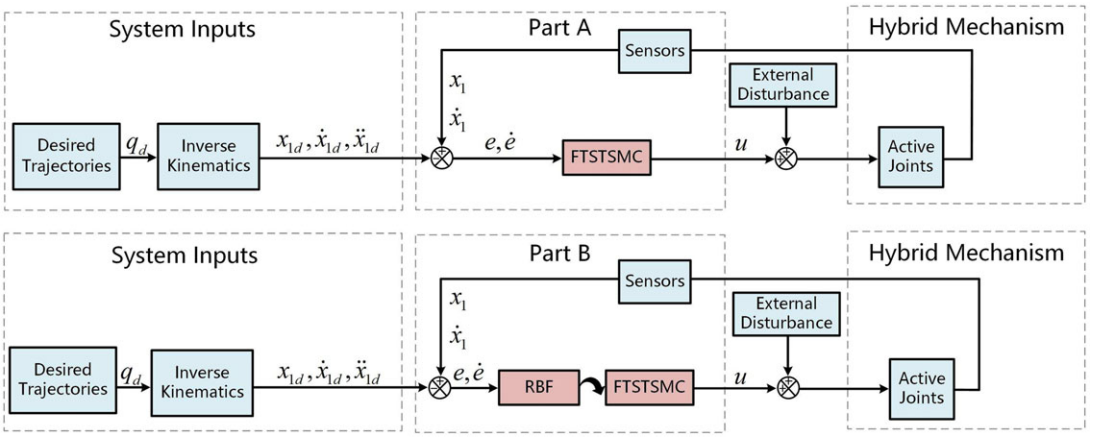

Figure 2. *The control schematic diagrams of FTSTSMC and IFTSTSMC for the uncertain hybrid mechanism.*

Lemma 2. [35] *If there is a continuous radial bounded function* $V{:}R^n \to R_+ \cup \{0\}$ *satisfying*

$$V(x) \le -\varphi_1 V^P(x) - \varphi_2 V^Q(x) + \eta_0$$

where $\varphi_1, \varphi_2 > 0$, $P > 1$, $0 < Q < 1$, *then the system (6) is said to be real fixed-time stable, and its convergence time T satisfies*

$$T \le T_{max} := \frac{1}{\varphi_1 \bar{\phi}(P-1)} + \frac{1}{\varphi_2 \bar{\phi}(1-Q)}$$

where $\bar{\phi}$ *is a positive constant and satisfies* $0 < \bar{\phi} < 1$, *the residual set of the solution of system (6) is*

$$x \in \left\{ x | V(x) \le \min \left\{ \left(\frac{\eta_0}{(1-\bar{\phi})\varphi_1} \right)^{\frac{1}{P}}, \left(\frac{\eta_0}{(1-\bar{\phi})\varphi_2} \right)^{\frac{1}{Q}} \right\} \right\}$$

Figure 2 presents the control schematic diagrams. As shown in Figure 2, first of all, the hybrid mechanism system is controlled under the designed FTSTSMC controller (Part A). Then, on this basis, RBF neural network is introduced to construct IFTSTSMC controller (Part B) to completely replace FTSTSMC controller (Part A).

3. Design of control algorithms

3.1. Fixed-time super-twisting sliding mode control

Let the sliding surface be

$$s = \dot{e} + \mathrm{sig}^{\alpha}(e) + \mathrm{sig}^{\beta}(e) \tag{7}$$

where $0 < \alpha < 1$, $1 < \beta$, $s = (s_1, \cdots, s_6)^T$.

To compute the derivative of s

$$\dot{s} = \ddot{e} + \alpha |e|^{\alpha-1} \dot{e} + \beta |e|^{\beta-1} \dot{e} \tag{8}$$

since

$$\begin{aligned} \ddot{e} &= \ddot{x}_1 - \ddot{x}_{1d} \\ &= \dot{x}_2 - \ddot{x}_{1d} \\ &= f(x) + g(x)u + D(x) - \ddot{x}_{1d} \end{aligned} \tag{9}$$

then

$$\dot{s} = f(x) + g(x)u + D(x) - \ddot{x}_{1d} + \alpha|e|^{\alpha-1}\dot{e} + \beta|e|^{\beta-1}\dot{e} \tag{10}$$

Based on the super-twisting algorithm, the following control law is designed

$$\begin{cases} \dot{s} = -k_1 \mathrm{sig}^{\frac{1}{2}}(s) - k_3 \mathrm{sig}^{\frac{3}{2}}(s) + w \\ \dot{w} = -k_2 \mathrm{sig}^{\frac{1}{2}}(s) + k_4 \mathrm{sig}^{\frac{3}{2}}(s) \end{cases} \tag{11}$$

Combining (5), (9), (10), and the following controller is designed

$$u = -g^{-1}(x)[f(x) - \ddot{x}_{1d} + \alpha|e|^{\alpha-1}\dot{e} + \beta|e|^{\beta-1}\dot{e} + \rho \mathrm{sign}(s) + k_1 \mathrm{sig}^{\frac{1}{2}}(s) + k_3 \mathrm{sig}^{\frac{3}{2}}(s) - w] \tag{12}$$

where $\rho \geq \delta$, $k_1, k_2, k_3, k_4 > 0$ is the design parameters to be determined.

Theorem 1. *If Assumption 1 is true, the super-twisting second-order sliding mode dynamic control law designed by (12) is adopted for the dynamic control system of hybrid mechanism (5), then the sliding mode surface s and $\dot{s}$ designed based on tracking error can converge to the origin within a fixed-time.*

Proof. Selecting Lyapunov function

$$V = \eta^T \mathbf{B} \eta \tag{13}$$

where $\eta = [|s|^{\frac{3}{2}}\mathrm{sign}(s), s, w]$, $\mathbf{B}$ is a symmetric positive definite matrix, defined as

$$\mathbf{B} = \frac{1}{2}\begin{bmatrix} 4k_2 + k_1^2 & k_1k_3 & -k_1 \\ k_1k_3 & 2k_4 + k_3^2 & -k_3 \\ -k_1 & -k_3 & \dfrac{k_1k_3}{k_2} \end{bmatrix}$$

The derivative of equation (13) is obtained

$$\begin{aligned} \dot{V} &= 2\eta^T \mathbf{B} \dot{\eta} \\ &= |s|^{\frac{5}{2}}\left[-\frac{3}{2}k_1\left(4k_2 + k_1^2\right) - k_3\left(2k_4 + k_3^2\right) - k_3k_4\right] + |s|^2\left[-\frac{5}{2}k_1^2k_3 + k_1k_2\right] \\ &+ |s|w\left[\frac{3}{2}k_1 + \left(2k_4 + k_3^2\right)\right] - \frac{3}{2}k_3\left(4k_2 + k_1^2\right)|s|^{\frac{7}{2}} + |s|^3\left[-\frac{3}{2}k_1k_3 - k_1k_3^2 - k_1k_4\right] \\ &+ |s|^2w\left[\frac{3}{2}k_1k_3 + \frac{3}{2}\left(4k_2 + k_1^2\right)\right] + |s|^{\frac{3}{2}}w\left[\frac{3}{2}k_1k_3 + k_3^2 + k_1k_3 + 2k_4\right] \\ &- \frac{3}{2}k_1|s|^{\frac{1}{2}}w^2 + |s|^{\frac{3}{2}}\left[-k_1\left(2k_4 + k_3^2\right) + k_2k_3\right] - k_3w^2 \\ &= -|s|^{-\frac{5}{2}}\left(\eta^T\mathbf{T_1}\eta\right)\left(\eta^T\mathbf{T_1}\eta\right)^T - |s|^{-\frac{3}{2}}\eta^T\mathbf{T_2}\eta - |s|^{\frac{1}{2}}\eta^T\mathbf{T_3}\eta - \eta^T\mathbf{T_4}\eta \end{aligned} \tag{14}$$

where $\mathbf{T_1}$, $\mathbf{T_2}$, $\mathbf{T_3}$, $\mathbf{T_4}$ are symmetric positive definite matrices. □

Since $|s|^{\frac{3}{2}} \leq \|\eta\|_2 \leq \left(\frac{V}{\lambda_{\min}(\mathbf{B})}\right)^{\frac{1}{2}}$, $|s|^{\frac{5}{2}} \leq \|\eta\|_2^{\frac{5}{3}} \leq \left(\frac{V}{\lambda_{\min}(\mathbf{B})}\right)^{\frac{5}{6}}$. Therefore, it follows that

$$\begin{aligned} \dot{V} &\leq -\frac{(\lambda_{\min}(\mathbf{B}))^{\frac{5}{6}}(\lambda_{\min}(\mathbf{T_1}))^2}{V^{\frac{5}{6}}}\frac{V^2}{(\lambda_{\max}(\mathbf{B}))^2} - \frac{(\lambda_{\min}(\mathbf{B}))^{\frac{1}{2}}\lambda_{\min}(\mathbf{T_2})}{V^{\frac{1}{2}}}\frac{V}{\lambda_{\max}(\mathbf{B})} \\ &= -\frac{(\lambda_{\min}(\mathbf{B}))^{\frac{5}{6}}(\lambda_{\min}(\mathbf{T_1}))^2}{(\lambda_{\max}(\mathbf{B}))^2}V^{\frac{7}{6}} - \frac{(\lambda_{\min}(\mathbf{B}))^{\frac{1}{2}}\lambda_{\min}(\mathbf{T_2})}{\lambda_{\max}(\mathbf{B})}V^{\frac{1}{2}} \end{aligned} \tag{15}$$

According to Lemma 1, the sliding surface s and $\dot{s}$ can converge to the origin in fixed-time T, that is, the system (5) can achieve stability in fixed-time T, and the convergence time is estimated as

$$T \leq \frac{6(\lambda_{\max}(\mathbf{B}))^2}{(\lambda_{\min}(\mathbf{B}))^{\frac{5}{6}}(\lambda_{\min}(\mathbf{T_1}))^2} + \frac{2\lambda_{\max}(\mathbf{B})}{(\lambda_{\min}(\mathbf{B}))^{\frac{1}{2}}\lambda_{\min}(\mathbf{T_2})} \tag{16}$$

Remark 1. The convergence time of finite-time sliding mode control (FTSMC) is related to the initial conditions of the system. However, the initial conditions of the actual hybrid mechanism may be difficult to obtain accurately in advance. In order to solve this problem, sliding mode surface (7) and control law (11) are designed on the basis of Lemma 1. The fixed-time performance parameters satisfying the conditions $P > 1$ and $0 < Q < 1$ are introduced into sliding variables and the transcendental function of the super-twisting algorithm respectively, so that the contraction of Lyapunov function can be applied to the form of lemma. Therefore, the global fixed-time convergence of the system is guaranteed.

Remark 2. The existence of sliding mode must be guaranteed during the implementation of SMC. It is worth noting that a sliding mode does exist on a discontinuity surface whenever the distances to this surface and the velocity of its change $\dot{s}$ are of opposite signs [36], that is, $\lim_{s\to 0^+} \dot{s} < 0$, $\lim_{s\to 0^-} \dot{s} > 0$. Therefore, Utkin was the first to propose sufficient conditions for the existence of sliding modes: $\lim_{s\to 0^+} \dot{s} \le 0$, $\lim_{s\to 0^-} \dot{s} \ge 0$, also known as the local reachability condition [37]. Further, if the condition $s\dot{s} \le 0$ is satisfied, it is called the global reachability condition of the sliding mode. According to the analysis of Theorem 1, the SMC designed in this paper satisfies the global reachability condition. Therefore, controller u needs to find u^- and u^+ to ensure that the system state variables can continue sliding along $s = 0$ when it reaches the sliding mode surface s. According to (5), u^- and u^+ should be satisfied that $g(x)u^+ < -\min(x_2 + D(x) + f(x))$, $g(x)u^- > -\max(x_2 + D(x) + f(x))$. It can be seen from the above that the boundary of the system uncertainty δ determines the realization of u to ensure the robustness of the SMC for the uncertain hybrid mechanism. Therefore, when the uncertainty parameter of the system exceeds δ, the SMC of the system will collapse. In order to avoid the limitation of this control, this paper will further introduce RBF neural network to deal with the control problem of the system with a wide range of uncertainties.

Remark 3. From the design viewpoint of the FTSTSMC, the method of literature [33] (FTSTSMC-1) can only achieve fixed-time convergence in the reaching stage of SMC. When it is applied to the hybrid mechanism, the sliding phase of SMC is greatly affected by the initial information of the system. Compared with FTSTSMC-1, the method designed in this paper (FTSTSMC) achieves fixed-time convergence in both reaching stage and sliding stage of SMC by adding the exponential power terms with the fixed-time performance parameters in sliding variables and the transcendental function of the super-twisting algorithm. Therefore, FTSTSMC achieves the global convergence performance of the system and overcomes the limitation that the sliding phase of FTSTSMC-1 is greatly affected by the initial information of the system.

3.2. Intelligent fixed-time super-twisting sliding mode control

RBF neural network [38] is a neural network for local approximation proposed by J. Moody and C. Darken in the late 1980s. It can approximate any nonlinear function and deal with the law that is difficult to analyze in the system. In (5), $F(x) = f(x) + D(x)$ is designed to be an unknown nonlinear function of the system, where $r(x)$ represents the load variation in $D(x)$. The uncertainty and unknown nature of $F(x)$ make it challenging to ensure the realization of the control law u. Therefore, RBF neural network is introduced to improve the adaptability of the system to the uncertainties with a wide range of changes.

RBF neural network is a forward-oriented network composed of three-layer networks.

The first layer: input layer, $x = [x_1, \cdots, x_n]^T$ is the input of the network, and n represents the number of dimensions of the input.

The second layer: the implicit layer, the output is $h(x) = [h_1, \cdots, h_m]^T$. Using the Gaussian basis function as the membership function of the input layer, that is,

$$h_j(x) = exp\left(-\frac{\|x - c\|^2}{2b^2}\right)$$

where c is the coordinate vector of the centroid of the Gaussian basis function in the implicit layer, b is the width of the Gaussian basis function in the implicit layer, $j = 1, \cdots, m$. The RBF neural network weight is $W = [W_1, \cdots, W_m]^T$.

The third layer: the output layer, the output of the neural network is $y = W^T h(x)$.

The RBF neural network is used to approximate $F(x)$, and the ideal output of the neural network is given as

$$F(x) = W^{*T} h(x) - \varepsilon$$

where W^* is the ideal weight of the RBF neural network, $h(x)$ is the output of the Gaussian function, and ε is the approximation error of the network. Let the actual output of the neural network be

$$\hat{f}(x) = \hat{W}^T h(x)$$

where $\hat{W}$ is the actual weight of the neural network. Defining $\tilde{W} = W^* - \hat{W}$, $\tilde{f}(x) = F(x) - \hat{f}(x)$, where $\tilde{W}$ is the error between the ideal weight and the actual weight, and $\tilde{f}(x)$ is the error between the ideal output and the actual output, so the fixed-time sliding mode controller based on RBF neural network can be designed as

$$u = -g^{-1}(x)\left[\hat{f}(x) - \ddot{x}_{1d} + \alpha|e|^{\alpha-1}\dot{e} + \beta|e|^{\beta-1}\dot{e} + k_1 \mathrm{sig}^{\frac{1}{2}}(s) + k_3 \mathrm{sig}^{\frac{3}{2}}(s) - w\right] \tag{17}$$

Then, the control law based on the super-twisting algorithm is

$$\begin{cases} \dot{s} = -k_1 \mathrm{sig}^{\frac{1}{2}}(s) - k_3 \mathrm{sig}^{\frac{3}{2}}(s) + w + \tilde{W}^T h(x) - \varepsilon \\ \dot{w} = k_2 \mathrm{sig}^{\frac{1}{2}}(s) - k_4 \mathrm{sig}^{\frac{3}{2}}(s) \end{cases} \tag{18}$$

Theorem 2. *If Assumption 1 is true, for the dynamic control system of hybrid mechanism (5), the intelligent super-twisting second-order sliding mode dynamic control law designed by (17) is adopted. Then the sliding mode surface s and $\dot{s}$ designed based on tracking error can converge to the origin within a real fixed-time.*

Proof. Selecting Lyapunov function

$$V_2 = \eta^T \mathbf{B} \eta \tag{19}$$

where $\eta = [|s|^{\frac{3}{2}}\mathrm{sign}(s), w, \tilde{W}]$, $\mathbf{B}$ is a symmetric positive definite matrix, defined as

$$\mathbf{B} = \frac{1}{2}\begin{bmatrix} 4k_2 + k_1^2 & k_1 k_3 & -k_1 \\ k_1 k_3 & 2k_4 + k_3^2 & -k_3 \\ -k_1 & -k_3 & 2 \end{bmatrix}$$

The derivative of equation (19) is obtained

$$\begin{aligned} \dot{V}_2 =& 2\eta^T \mathbf{B} \dot{\eta} \\ =& -6k_1\left(k_2 + k_1^2\right)|s|^{\frac{5}{2}} - 6k_3\left(k_2 + k_1^2\right)|s|^{\frac{7}{2}} - 6\left(k_2 + k_1^2\right)|s|^2 w + 6\left(k_2 + k_1^2\right)|s|^2 \\ & \times \tilde{W}^T h(x) - 6\left(k_2 + k_1^2\right)|s|^2 \varepsilon - \frac{3}{2}k_1^2 k_3 |s| w - \frac{3}{2}k_1 k_3^2 |s|^2 w + \frac{3}{2}k_1 k_3 |s|^{\frac{1}{2}} w^2 \\ & + \frac{3}{2}k_1 k_3 |s|^{\frac{1}{2}} w \tilde{W}^T h(x) - \frac{3}{2}k_1 k_3 |s|^{\frac{1}{2}} w\varepsilon + \frac{3}{2}k_1^2 \tilde{W}|s| + \frac{3}{2}k_1 k_3 \tilde{W}|s|^2 - \frac{3}{2}k_1 \\ & \times |s|^{\frac{1}{2}} w\tilde{W} - \frac{3}{2}k_1 |s|^{\frac{1}{2}} \tilde{W}\tilde{W}^T h(x) + \frac{3}{2}k_1 |s|^{\frac{1}{2}} \tilde{W}\varepsilon + k_1 k_2 k_3 |s|^2 - k_1 k_3 k_4 |s|^3 \\ & + k_2(2k_4 + k_3^2)|s|^{\frac{1}{2}} w - k_4(2k_4 + k_3^2)|s|^{\frac{3}{2}} w - k_2 k_3 \tilde{W}|s|^{\frac{1}{2}} + k_3 k_4 \tilde{W}|s|^{\frac{3}{2}} \\ & - k_1 |s|^{\frac{3}{2}} \dot{\tilde{W}} - k_3 w\dot{\tilde{W}} + 2\tilde{W}\dot{\tilde{W}} \\ \leq& -|s|^{-\frac{5}{2}}(\eta^T \mathbf{T_5} \eta)(\eta^T \mathbf{T_5} \eta)^T - |s|^{-\frac{1}{2}} \eta^T \mathbf{T_6} \eta - |s|^{\frac{1}{2}} \eta^T \mathbf{T_7} \eta - \eta^T \mathbf{T_8} \eta + \eta_0 \end{aligned} \tag{20}$$

where $\varepsilon = 0$ is negligible, $\eta_0 > 0$, $\dot{\tilde{W}} = -3\left(k_2 + k_1^2\right)|s|^2 h(x)$, and $\mathbf{T_5}$, $\mathbf{T_6}$, $\mathbf{T_7}$, $\mathbf{T_8}$ are symmetric positive definite matrices. □

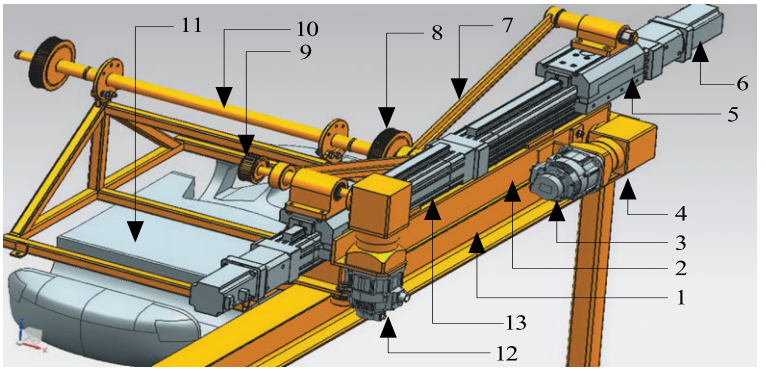

1. The guide rail 2. The base 3.The driving motor of the walking mechanism 4. The gear reducer 5. The slider 6. The driving motor of the lifting mechanism 7. The link 8. The driven wheel 9. The driving wheel 10.The connecting rod 11. The car body 12. The driving motor of the turning mechanism 13. The screw.

Figure 3. *Structure of hybrid mechanism system (single side).*

Since $|s|^{\frac{3}{2}} \le \|\eta\|_2 \le \left(\frac{V_2}{\lambda_{\min}(\mathbf{B})}\right)^{\frac{1}{2}}$, $|s|^{\frac{1}{2}} \le \|\eta\|_2^{\frac{1}{3}} \le \left(\frac{V_2}{\lambda_{\min}(\mathbf{B})}\right)^{\frac{1}{6}}$, $|s|^{\frac{5}{2}} \le \|\eta\|_2^{\frac{5}{3}} \le \left(\frac{V_2}{\lambda_{\min}(\mathbf{B})}\right)^{\frac{5}{6}}$.

Therefore, it follows that

$$\begin{aligned}\dot{V}_2 &\le -\frac{(\lambda_{\min}(\mathbf{B}))^{\frac{5}{6}}}{V_2^{\frac{5}{6}}}(\lambda_{\min}(\mathbf{T_5}))^2\frac{V_2^2}{(\lambda_{\max}(\mathbf{B}))^2} - \frac{(\lambda_{\min}(\mathbf{B}))^{\frac{1}{6}}}{V_2^{\frac{1}{6}}}\lambda_{\min}(\mathbf{T_6})\frac{V_2}{\lambda_{\max}(\mathbf{B})} + \eta_0 \\ &= -\frac{(\lambda_{\min}(\mathbf{B}))^{\frac{5}{6}}(\lambda_{\min}(\mathbf{T_5}))^2}{(\lambda_{\max}(\mathbf{B}))^2}V_2^{\frac{7}{6}} - \frac{(\lambda_{\min}(\mathbf{B}))^{\frac{1}{6}}\lambda_{\min}(\mathbf{T_6})}{\lambda_{\max}(\mathbf{B})}V_2^{\frac{5}{6}} + \eta_0 \end{aligned} \tag{21}$$

According to Lemma 2, the sliding mode surface s and $\dot{s}$ can converge to the origin in the real fixed-time $\bar{T}$, that is, the system (5) can achieve stability in the real fixed-time $\bar{T}$, and the estimated convergence time is

$$\bar{T} \le \frac{6(\lambda_{\max}(\mathbf{B}))^2}{\lambda_{\min}(\mathbf{B}))^{\frac{5}{6}}(\lambda_{\min}(\mathbf{T_5}))^2\bar{\phi}} + \frac{6\lambda_{\max}(\mathbf{B})}{(\lambda_{\min}(\mathbf{B}))^{\frac{1}{6}}\lambda_{\min}(\mathbf{T_6})\bar{\phi}} \tag{22}$$

And the system states converge to the following compact set Ω within the real fixed-time $\bar{T}$.

$$\Omega \in \left\{x|V_2(x) \le \min\left\{\left(\frac{\eta_0(\lambda_{\max}(\mathbf{B}))^2}{(1-\bar{\phi})(\lambda_{\min}(\mathbf{B}))^{\frac{5}{6}}(\lambda_{\min}(\mathbf{T}_5))^2}\right)^{\frac{6}{7}}, \left(\frac{\eta_0\lambda_{\max}(\mathbf{B})}{(1-\bar{\phi})(\lambda_{\min}(\mathbf{B}))^{\frac{1}{6}}\lambda_{\min}(\mathbf{T}_6)}\right)^{\frac{6}{5}}\right\}\right\}$$

4. Simulations

To verify the effectiveness of the proposed methods, the proposed method FTSTSMC is compared with FTSMC, and the proposed method IFTSTSMC is compared with FTSTSMC. Simulation comparisons are conducted with Matlab/Simulink.

The unilateral structure of the bilaterally symmetrical hybrid mechanism system is shown in Figure 3. The forward and backward movement of the hybrid mechanism system is driven by the walking wheels. The up-down and turnover movement is achieved by two symmetrical parallel mechanisms. The rack of the lifting and turning mechanism (LTM) is the motion part of the walking mechanism. Two sets of LTM are connected via a connecting rod and a fixed mount used to place the car body. The LTM consists of a lifting part fixed on the walking mechanism and a turning part fixed on the connecting rod. Via the combination of the walking mechanism and the LTM, the car body is driven to realize the forward and backward, up and down, turnover, and compound movement.

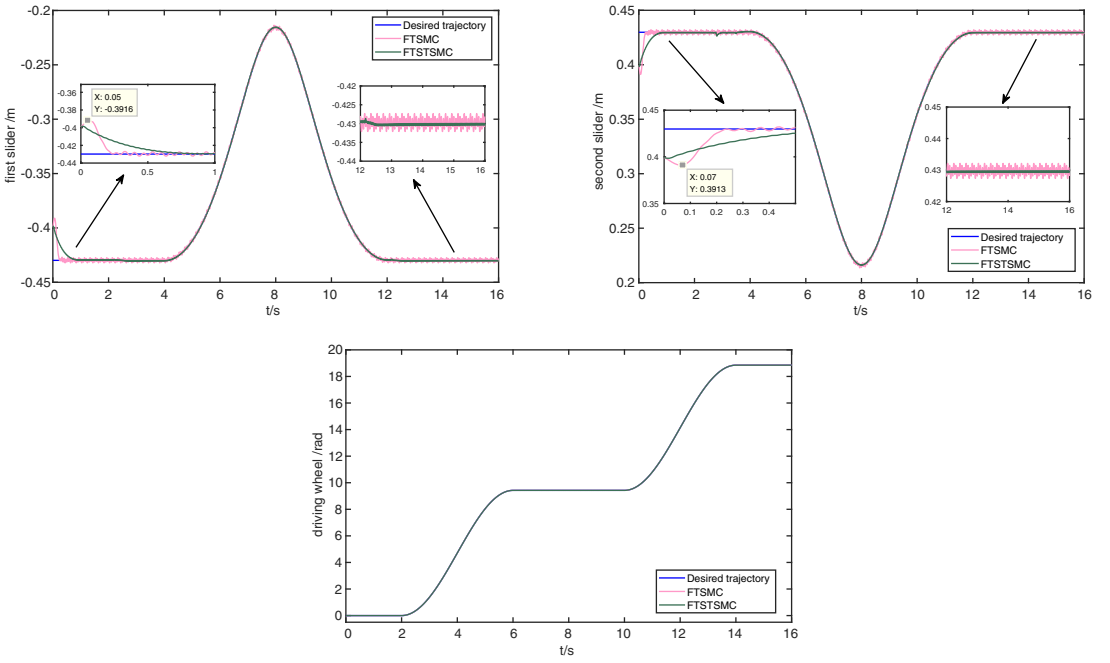

Figure 4. *Tracking trajectory curves of sliders and driving wheel.*

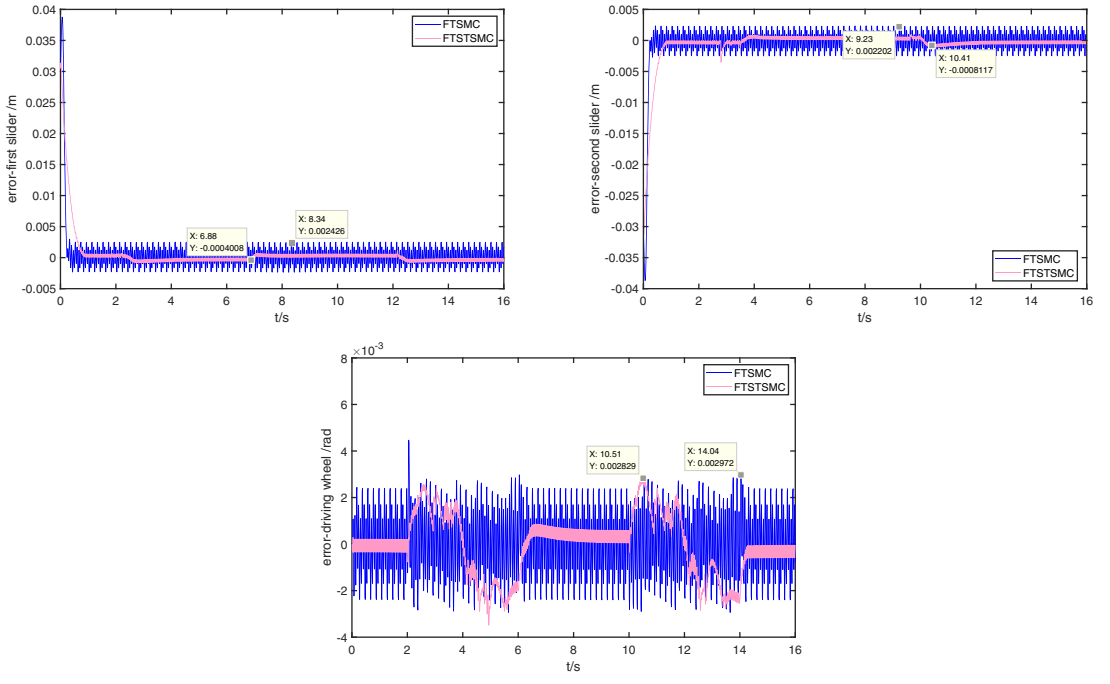

Figure 5. *Tracking error curves of sliders and driving wheel.*

In FTSTSMC, the parameters are respectively designed as $k_1 = 1.80$, $k_2 = 1.90$, $k_3 = 18.70$, $k_4 = 6.40$, $\rho = 2.00$, $\alpha = 0.66$, $\beta = 2.00$. The simulation results of FTSTSMC and FTSMC are as follows. Since the hybrid mechanism system has the characteristics of bilateral symmetry, the tracking trajectory curves and tracking error curves of sliders 1, 2 and driving wheel 1 are shown in Figure 4 and Figure 5,

Table I. *The RMSE and MASSE of the active joints for simulation experimental results.*

		FTSMC	FTSTSMC-1	FTSTSMC	IFTSTSMC
RMSE	**slider 1**	3.584×10^{-3}	3.231×10^{-3}	3.228×10^{-3}	2.156×10^{-3}
	slider 2	3.575×10^{-3}	3.210×10^{-3}	3.206×10^{-3}	2.152×10^{-3}
	driving wheel 1	1.450×10^{-3}	1.316×10^{-3}	1.290×10^{-3}	7.720×10^{-4}
MASSE	**slider 1**	2.426×10^{-3}	1.167×10^{-3}	4.008×10^{-4}	1.221×10^{-4}
	slider 2	2.202×10^{-3}	1.707×10^{-3}	8.117×10^{-4}	1.737×10^{-4}
	driving wheel 1	2.972×10^{-3}	4.784×10^{-3}	2.829×10^{-3}	2.791×10^{-3}

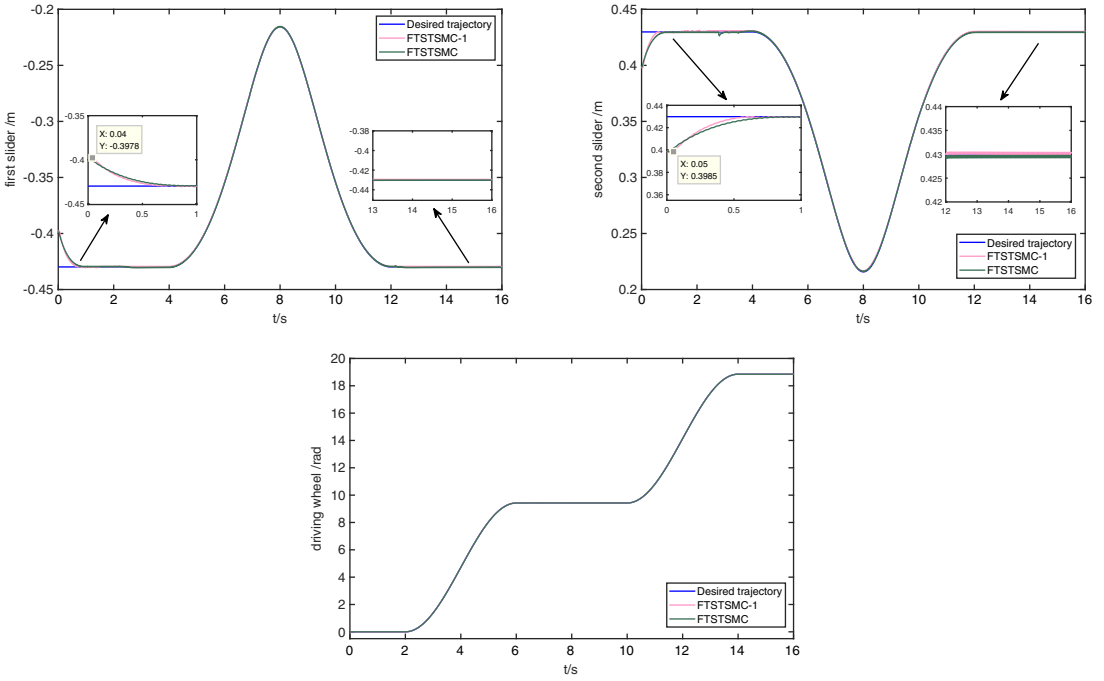

Figure 6. *Tracking trajectory curves of sliders and driving wheel.*

respectively. As seen in the partial block of Figure 4, the trajectory tracking curves of slider 1 and slider 2 for the hybrid mechanism system show the abrupt changes caused by the fluid resistance when entering into the tank. The values of the abrupt changes are $0.3916m$ and $0.3913m$, respectively, which affect the tracking accuracy and the control performance of the system. Compared to FTSMC, due to the fixed-time control with faster convergence performance and better robustness, FTSTSMC can reduce the abrupt changes caused when the hybrid mechanism system enters into the tank. In addition, the root mean square error (RMSE) and the maximum absolute steady-state error (MASSE) of the active joints are shown in Table I; it can be seen that the RMSE of the active joints for FTSTSMC is about 9.93%, 10.32%, and 11.03% reduced than FTSMC, respectively. And the MASSE of the active joints for FTSTSMC is about 83.47%, 63.14%, and 4.81% reduced than FTSMC, respectively. Therefore, FTSTSMC has better tracking accuracy.

From the design viewpoint of the FTSTSMC, compared with literature [33] (FTSTSMC-1), the method designed in this paper (FTSTSMC) has variable fixed-time performance parameters, and FTSTSMC achieves fixed-time convergence in both reaching stage and sliding stage of the SMC. Figure 6 and Figure 7 show the comparison results of the above two simulation experiments. Table I shows the RMSE and MASSE of the active joints for the controllers. It shows that the RMSE of the active joints for FTSTSMC is about 0.09%, 0.12%, and 1.98% reduced than FTSTSMC-1, respectively.

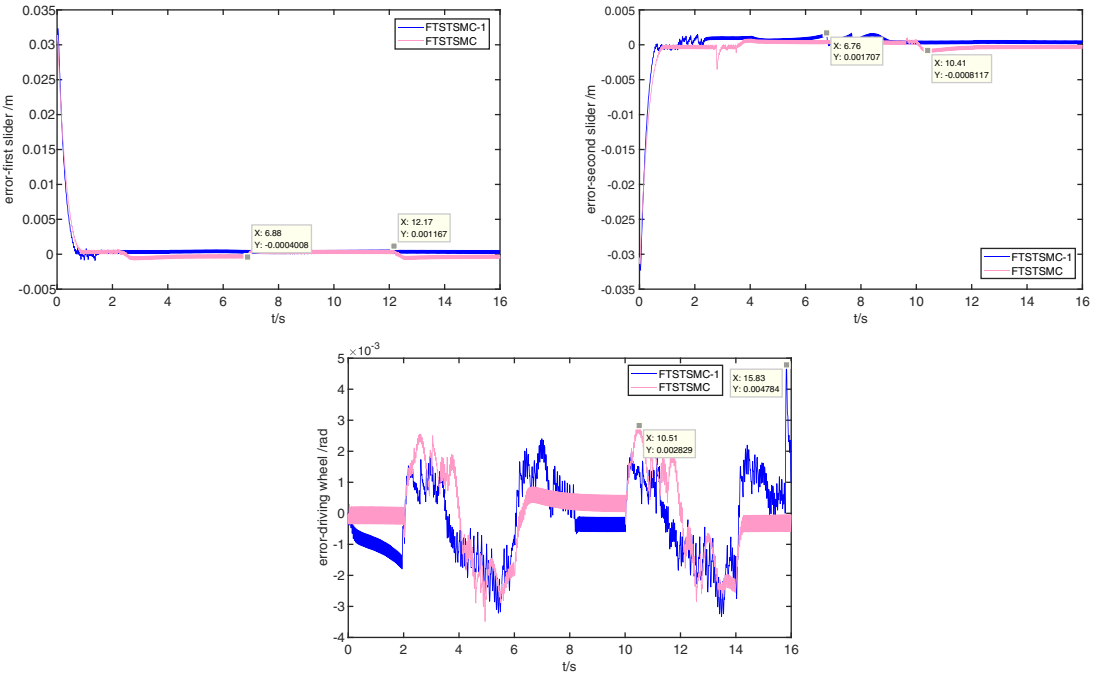

Figure 7. *Tracking error curves of sliders and driving wheel.*

The MASSE of the active joints for FTSTSMC is about 65.66%, 52.45%, and 40.87% reduced than FTSTSMC-1, respectively. Therefore, the FTSTSMC designed in this paper has better tracking effect.

However, it can be seen from Figure 4 and Figure 5 that the tracking effect of FTSTSCM has not been greatly improved and local chattering still exists. Therefore, IFTSTSCM is proposed in this paper. In the IFTSTSMC, the parameters are, respectively, designed as $k_1 = 3.00$, $k_2 = 2.30$, $k_3 = 56.69$, $k_4 = 229.54$, $\alpha = 0.52$, $\beta = 1.01$. The simulation results are shown in Figure 8 and Figure 9. It can be seen from the partial block of Figure 8 that the trajectory tracking curves for IFTSTSCM converges about 57.47% faster than FTSTSMC. Table I shows that the RMSE of the active joints for IFTSTSCM is about 33.21%, 32.88%, and 40.16% reduced than FTSTSMC, respectively. And the MASSE of the active joints for IFTSTSCM is about 69.54%, 78.60%, and 1.34% reduced than FTSTSMC, respectively. Therefore, compared with FTSTSMC, IFTSTSMC has better tracking effect. When the uncertainties of the hybrid mechanism change in a wide range, the existence condition of SMC is destroyed, resulting in the failure of the robustness for the FTSTSMC. IFTSTSMC introduces RBF neural network, which deals with nonlinear functions containing the inherent dynamics and uncertainties of the system. In order to break through the uncertainties range of FTSTSCM, the uncertainties are amplified by 10 times and 100 times for simulation experiments. Figure 10 and Figure 11 show the tracking curves and error tracking curves of the system after the uncertainties amplification. It can be seen that FTSTSCM can achieve system stability in response to uncertainties within a certain range. However, when faced with a wide range of uncertainties, it may lead to control failures. IFTSTSMC has a good adjustment effect on a wide range of uncertainties. It can not only make the system converge in real fixed-time but also improve the adaptability of the hybrid mechanism system to the uncertainties with a wide range of changes.

5. Prototype experiment

The prototype of hybrid mechanism system is shown in Figure 12. Figure 13 and Figure 14 show the time-series images of the hybrid mechanism pose in operation and the pose of the hybrid mechanism system in operation with the electrophoretic tank, respectively. The physical parameters of the prototype

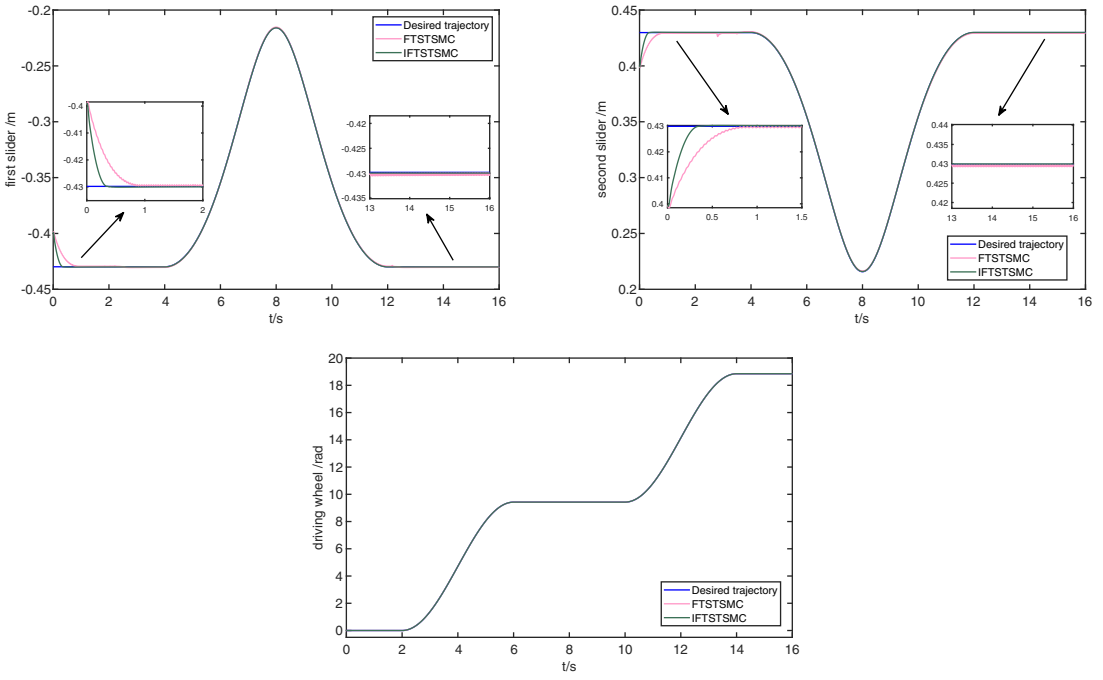

Figure 8. *Tracking trajectory curves of sliders and driving wheel.*

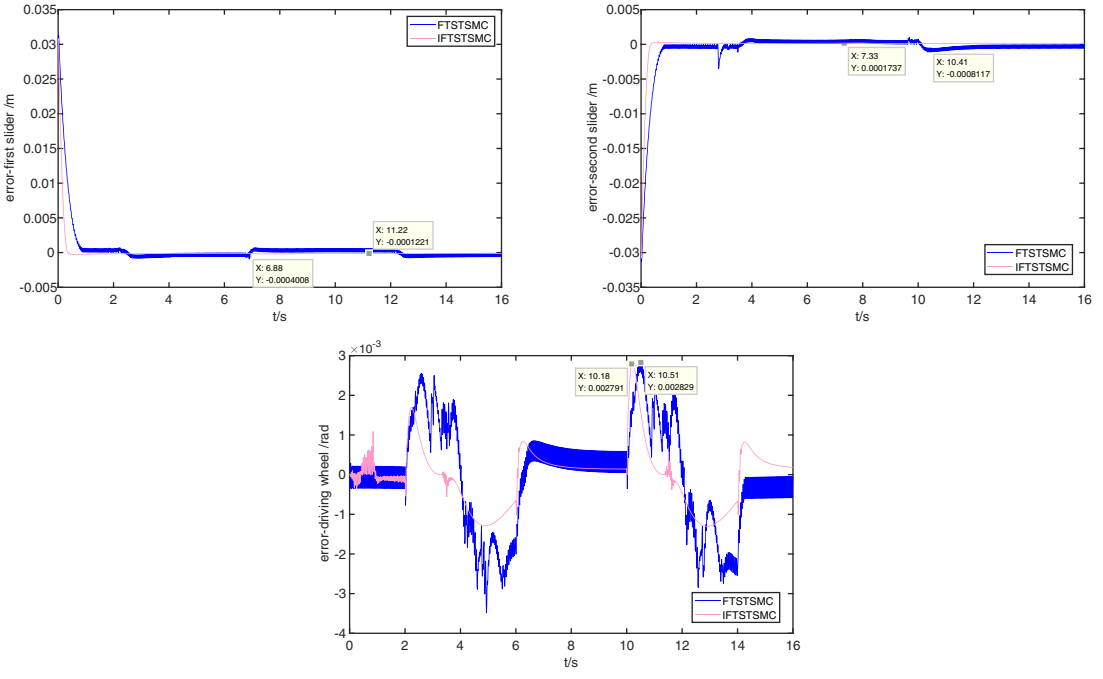

Figure 9. *Tracking error curves of sliders and driving wheel.*

include the length of the connecting rod is 0.495m, the length of the connecting rod is 0.72m, the lead of the lead screw is 0.01m, the radius of the active driving wheel is 0.025m, and the radius of the driven driving wheel is 0.075m. The control system is divided into three layers: upper computer (PC), lower

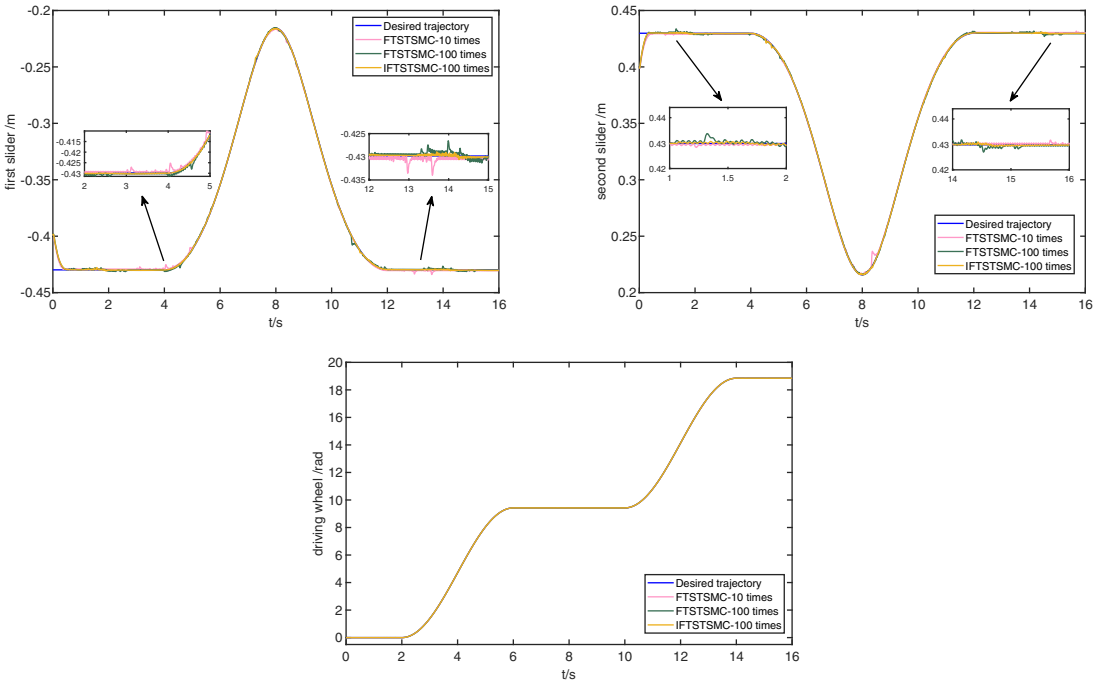

Figure 10. *Tracking trajectory curves of sliders and driving wheel with RBF neural network.*

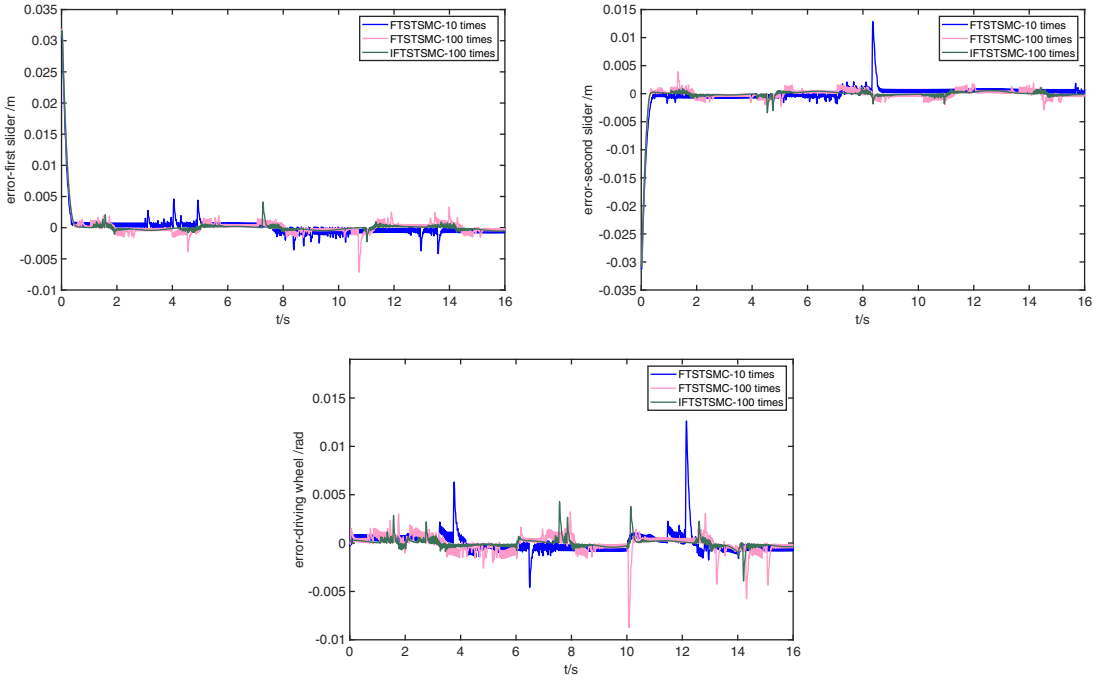

Figure 11. *Tracking error curves of sliders and driving wheel with RBF neural network.*

computer (UMAC), and servo drive system. Among them, the PC uses Intel Core i7-4790 3.60 GHz processor to complete the functions of the human-computer interaction, code initialization and compilation, and condition monitoring. The UMAC mainly includes a TURBO PMAC2 OPT-5C0 CPU main board,

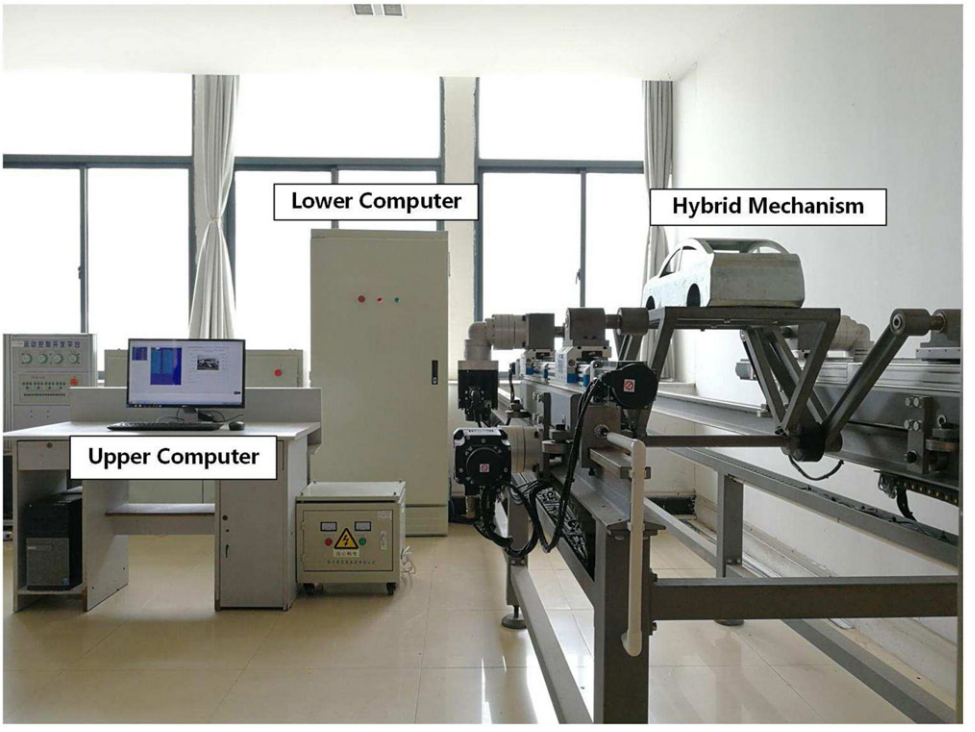

The prototype of the hybrid mechanism system in the figure mainly contains the upper computer, the lower computer and the hybrid mechanism. The upper computer is used to achieve human-computer interaction, program initialization and compilation, and operational state monitoring. The lower computer is used to accomplish data calculation, digital to analog conversion, and motion control.

Figure 12. *The prototype of hybrid mechanism system.*

tow AC-24E2A axis board, one AC-65E I/O board, and one AC-E1 power board. It is used to accomplish data calculation, digital to analog conversion, and motion control. The servo drive system is composed of MRJ4-70A(30W), MR-J4-100A(30W) servo drivers, and HG-KR73BJ(750W), HG-SR102BJ(30W) AC servo motors. The reducer is selected as EVH-115-20-K7-28HF24, and its reduction ratio is 1:20. To realize the feedback control loop of the system, the 22-bit (4194304pulses/rev) high-resolution absolute position encoder is selected. Based on the above setup, an experimental platform of the hybrid mechanism system for the automobile electro-coating conveying is constructed. The control algorithm is implemented as follows: opening the Pewin32 software to enable the PC to communicate with the UMAC; the AC servo motor is closed looped via Pewin32 software instruction and the motion trajectory program is downloaded to UMAC; opening the PC interface via VC++ 6.0(SP6) and downloading the control algorithm program into the UMAC; and running the designed control algorithm program.

Three contrast motion control experiments are carried out on the prototype. The control algorithm is realized by establishing the connection between PC and UMAC to open the closed loop of the system. Download the required tracks and user-defined motion programs precompiled by PeWin32pro software to the UMAC buffer. The results of the comparison experiments between FTSTSCM and FTSCM, FTSTSCM-1 and FTSTSCM, and FTSTSCM and IFTSTSCM are shown in Figure 15, Figure 16, and Figure 17, respectively. And the RMSE and MASSE of the comparison experiments are shown in Table II, where the RMSE of the active joints for FTSTSCM is about 59.26%, 59.28%, and 59.87% reduced than FTSMC; the MASSE of the active joints for FTSTSCM is about 60.55%, 62.25%, and

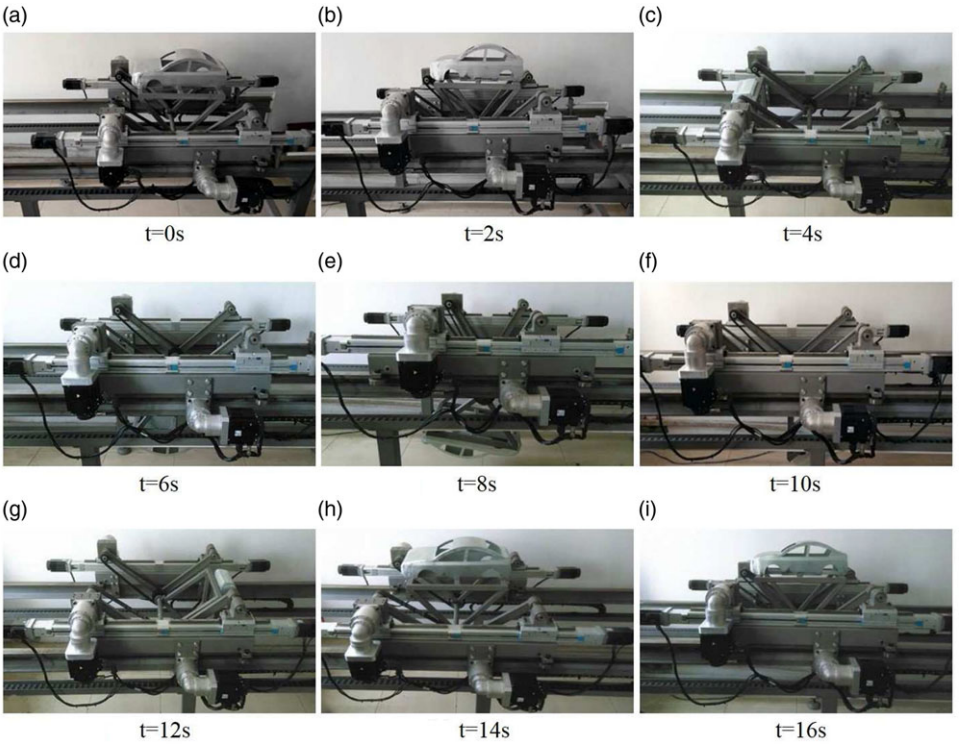

The pose of the hybrid mechanism used for automobile electro-coating conveying at different moments in the operation.

Figure 13. *Time-series images of the hybrid mechanism pose in operation.*

The operation of the hybrid mechanism system used for automobile electro-coating conveying is divided into three stages: entry into the tank, in-tank and out-tank. The lifting and turning mechanism perform the downward turning motion with an overall turning angle of 180 degrees to complete the motion of entry into the tank. In the tank, the walking mechanism moves in parallel to make the body in white of the automobile to carry out electro-coating in the fluid and the lifting and turning mechanism perform the small amplitude sinusoidal motion to solve the air packet problem. Finally, the lifting and turning mechanism perform a turning movement with an overall turning angle of 180 degrees to complete the coating conveying process.

Figure 14. *The pose of the hybrid mechanism system in operation with the electrophoretic tank.*

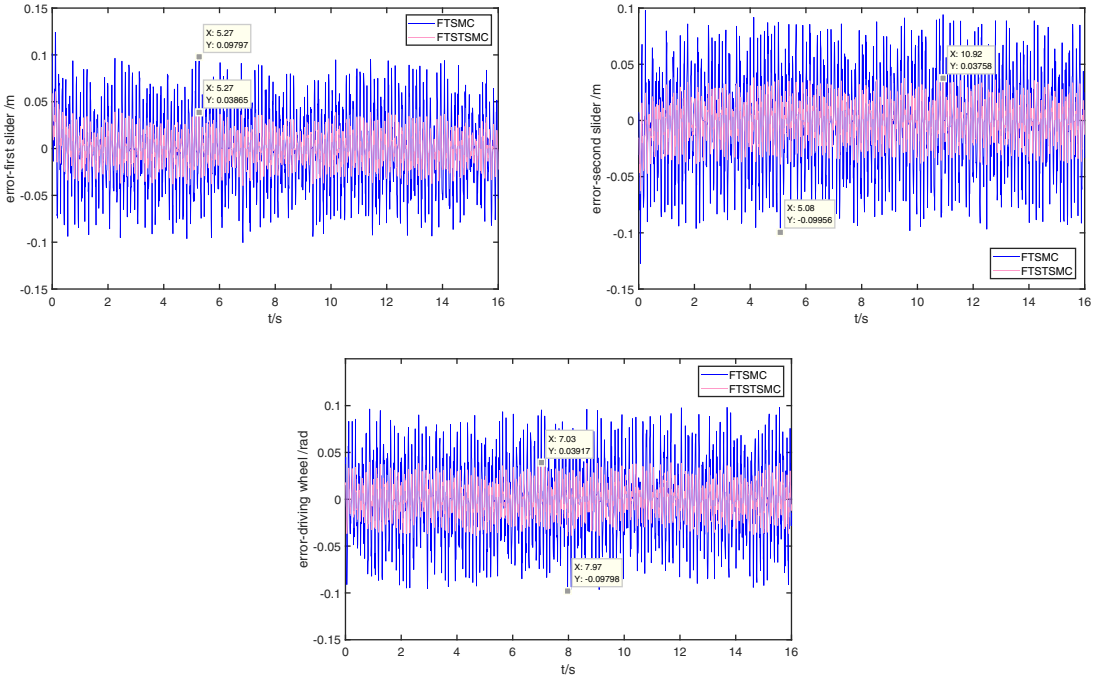

Figure 15. *Experimental results of tracking errors for FTSTSCM and FTSCM.*

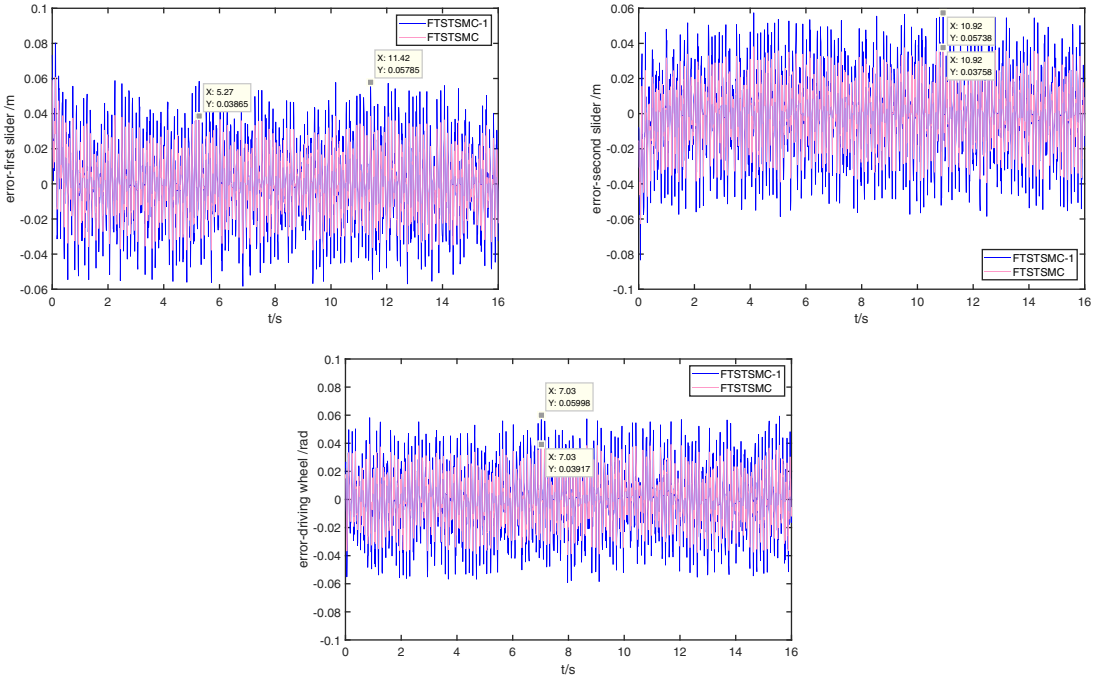

Figure 16. *Experimental results of tracking errors for FTSTSCM-1 and FTSTSCM.*

Table II. *The RMSE and MASSE of the active joints for prototype experimental results.*

		FTSMC	FTSTSMC-1	FTSTSMC	IFTSTSMC
RMSE	**slider 1**	4.058×10^{-2}	2.449×10^{-2}	1.653×10^{-2}	8.389×10^{-3}
	slider 2	4.138×10^{-2}	2.496×10^{-2}	1.685×10^{-2}	8.528×10^{-3}
	driving wheel 1	4.124×10^{-2}	2.481×10^{-2}	1.655×10^{-2}	8.292×10^{-3}
MASSE	**slider 1**	9.797×10^{-2}	5.785×10^{-2}	3.865×10^{-2}	1.876×10^{-2}
	slider 2	9.956×10^{-2}	5.738×10^{-2}	3.758×10^{-2}	1.886×10^{-2}
	driving wheel 1	9.798×10^{-2}	5.998×10^{-2}	3.917×10^{-2}	1.933×10^{-2}

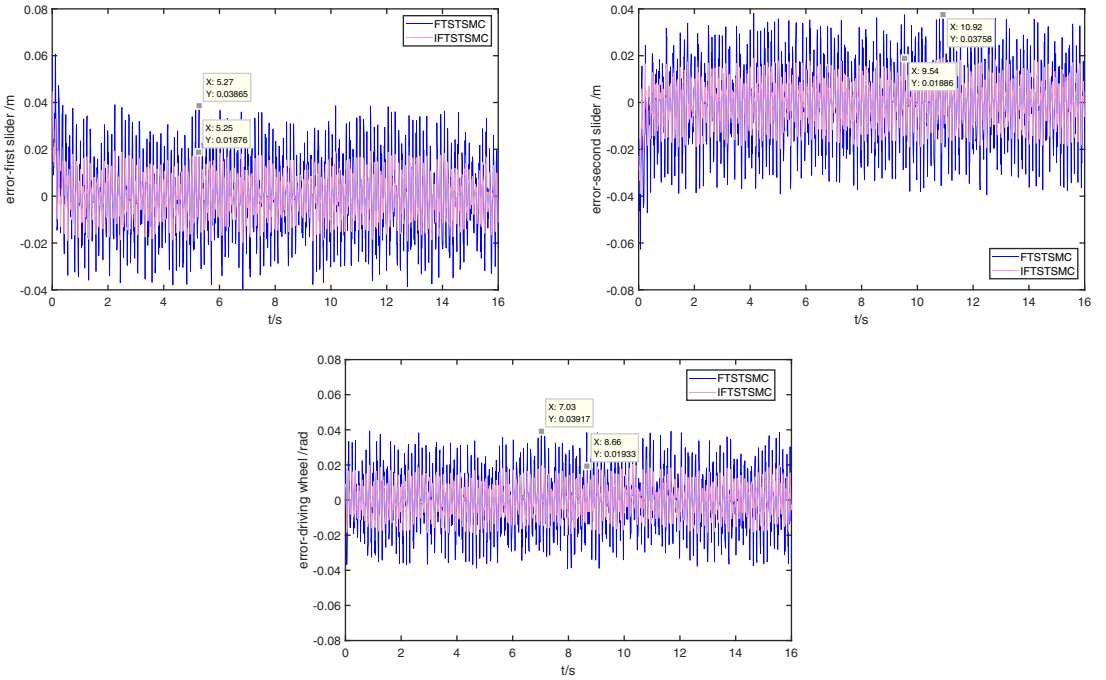

Figure 17. *Experimental results of tracking errors for FTSTSCM and IFTSTSCM.*

60.02% reduced than FTSMC; the RMSE of the active joints for FTSTSCM is about 32.50%, 32.49%, and 33.29% reduced than FTSTSCM-1; the MASSE of the active joints for FTSTSCM is about 33.19%, 34.51%, and 34.69% reduced than FTSTSCM-1; the RMSE of the active joints for IFTSTSCM is about 49.25%, 49.37%, and 49.89% reduced than FTSTSCM; and the MASSE of the active joints for IFTSTSCM is about 51.46%, 49.81%, and 50.65% reduced than FTSTSCM. Therefore, in general, the proposed control method can obtain better tracking control performance. As a nonlinear control method, IFTSTSMC can effectively deal with the uncertainties of the system, so it is excellent in enhancing the robustness of hybrid mechanism system to the uncertainties with a wide range of changes. In addition to the uncertain hybrid mechanisms, IFTSTSMC can be used in mechanical systems, power systems, aerospace systems, industrial production systems, and other practical systems. By designing the sliding mode surface and control law reasonably, IFTSTSMC can effectively achieve the stability and convergence of the system. In general, the method proposed in this paper is not only beneficial to the hybrid mechanism, but also has universal applicability to other practical systems. Therefore, this method is of great significance in engineering practice.

6. Conclusion

In this paper, in order to improve the global convergence performance of STSMC for the uncertain hybrid mechanism, the design idea of the fixed-time control is introduced into the STSMC. By adding the exponential power terms with the fixed-time performance parameters in sliding variables and the transcendental function of super-twisting algorithm, the convergence performance of STSMC in the reaching stage and sliding stage is improved, so as to achieve the global convergence of the uncertain hybrid mechanism system. Further, in order to enhance the robustness of hybrid mechanism system to the uncertainties with a wide range of changes, the existence condition of FTSTSMC for the uncertain hybrid mechanism is analyzed, and IFTSTSMC is designed by introducing RBF neural network. Finally, the effectiveness of the control method is verified by simulation and prototype experiments. In the future, we will further consider introducing deep learning method to enhance the intelligence of the uncertain hybrid mechanism system.

Author contributions. All authors contributed to the study conception and design. Initial material preparation and analysis were performed by Xue Li. The first draft of the manuscript was written by Xue Li and Guoqin Gao. All authors commented on previous versions of the manuscript. All authors read and approved the final manuscript.

Financial support. This work was supported by the National Natural Science Foundation of China (G.G., grant number 51375210); Zhenjiang Municipal Key Research and Development Program (G.G., grant number GZ2018004); Priority Academic Program Development of Jiangsu Higher Education Institutions (G.G., grant number PAPD-2022-5); and Jiangsu graduate research innovation program (X.L., grant number KYCX23_3680).

Competing interests. The authors declare no conflict of interest.

Ethical approval. None.

References

[1] X. Q. Lü, R. Y. Deng, X. Y. Li and Y. B. Wu, "Comprehensive performance evaluation and optimization of hybrid power robot based on proton exchange membrane fuel cell," *Int J Energy Res* **46**(2), 1934–1950 (2022).
[2] N. Natarajan, S. Vaitheswaran, M. R. Lima, M. Wairagkar and R. Vaidyanathan, "Acceptability of social robots and adaptation of hybrid-face robot for dementia care in india: A qualitative study," *Am J Geriatr Psychiatry* **30**(2), 240–245 (2022).
[3] Y. Zhang, H. Li, X. Qin, J. liu and Z. Hou, "Analysis of vibration response and machining quality of hybrid robot based UD-CFRP trimming," *Proc Inst Mech Eng B J Eng Manuf* **235**(6-7), 974–986 (2021).
[4] S. Yu, J. Puchinger and S. Sun, "Van-based robot hybrid pickup and delivery routing problem," *European J Oper Res* **298**(3), 894–914 (2022).
[5] Q. Chen, B. Zi, Z. Sun, Y. Li and Q. S. Xu, "Design and development of a new cable-driven parallel robot for waist rehabilitation," *IEEE/ASME Trans Mechatron* **24**(4), 1497–1507 (2019).
[6] F. Gao, X. Liu and W. A. Gruver, "Performance evaluation of two-degree-of-freedom planar parallel robots," *Mech Mach Theory* **33**(6), 661–668 (1998).
[7] A. Ghasemi, F. Parivash and S. Ebrahimian, "Autonomous landing of a quadrotor on a moving platform using vision-based FOFPID control," *Robotica* **40**(5), 1431–1449 (2022).
[8] Z. Li, Y. Yang and S. Wang, "Adaptive dynamic coupling control of hybrid joints of human-symbiotic wheeled mobile manipulators with unmodelled dynamics," *Int J Soc Robot* **2**(2), 109–120 (2010).
[9] K. D. Do, "Global inverse optimal exponential path-tracking control of mobile robots driven by Levy processes," *Robotica* **39**(12), 2306–2332 (2021).
[10] K. Naseri, M. T. Vu, S. Mobayen, A. Najafi and A. Fekih, "Design of linear matrix inequality-based adaptive barrier global sliding mode fault tolerant control for uncertain systems with faulty actuators," *Mathematics* **10**(13), 2159 (2022).
[11] A. Naderolasli, K. Shojaei and A. Chatraei, "Terminal sliding-mode disturbance observer-based finite-time adaptive-neural formation control of autonomous surface vessels under output constraints," *Robotica* **41**(1), 236–258 (2023).
[12] X. Yang, H. T. Liu, J. L. Xiao, W. L. Zhu, Q. Liu, G. F. Gong and T. Huang, "Continuous friction feedforward sliding mode controller for a trimule hybrid robot," *IEEE/ASME Trans Mechatron* **23**(4), 1673–1683 (2018).
[13] Q. Y. Qin and G. Q. Gao, "Composite error-based intelligent adaptive sliding mode control for uncertain bilaterally symmetrical hybrid robot with variational desired trajectories," *Appl Sci* **11**(6), 2613 (2021).
[14] R. Kikuuwe, R. Pasaribu and G. Byun, "A first-order differentiator with first-order sliding mode filtering," *IFAC-PapersOnLine* **52**(16), 771–776 (2019).

[15] M. A. E. Alali and J.-P. Barbot, "A first order sliding mode controller for grid connected shunt active filter with a LCL filter," *IFAC-PapersOnLine* **50**(1), 14812–14817 (2017).
[16] R. G. Roy and D. Ghoshal, "Grey wolf optimization-based second order sliding mode control for inchworm robot," *Robotica* **38**(9), 1539–1557 (2020).
[17] J. Wu, H. T. Zhu and X. D. Li, "Time-varying second-order sliding mode control for systems subject to external disturbance," *IEEE Access* **8**, 183344–183350 (2020).
[18] J. C. Chen, Z. B. Shuai, H. Zhang and W. Z. Zhao, "Path following control of autonomous four-wheel-independent-drive electric vehicles via second-order sliding mode and nonlinear disturbance observer techniques," *IEEE Trans Ind Electron* **68**(3), 2460–2469 (2020).
[19] L. Sha and S. B. Wang, "High-order sliding-mode control of two-inertia system based on disturbance observer," *Control Eng China* **28**(4), 724–729 (2021).
[20] J. Zhang, W. J. Meng, Y. F. Yin, Z. N. Li and W. Q. Liang, "High-order sliding mode control for three-joint rigid manipulators based on an improved particle swarm optimization neural network," *Mathematics* **10**(19), 3418 (2022).
[21] A. Chandra and P. Lal, "Higher order sliding mode controller for a quadrotor UAV with a suspended load," *IFAC-PapersOnLine* **55**(1), 610–615 (2022).
[22] J. K. Goyal, S. Kamal, R. B. Patel, X. H. Yu, J. P. Mishra and S. Ghosh, "Higher order sliding mode control-based finite-time constrained stabilization," *IEEE Trans Circuits Syst II Exp Briefs* **67**(2), 295–299 (2020).
[23] A. Levant, "Chattering analysis," *IEEE Trans Automat Control* **55**(6), 1380–1389 (2010).
[24] V. Mien, F. Pasquale and C. Dariusz, "Fault diagnosis and fault-tolerant control of uncertain robot manipulators using high-order sliding mode," *Math Probl Eng Theory Meth Appl* **2016**(9), 1–14 (2016).
[25] H. Y. Jia, W. W. Shang, F. Xie, B. Zhang and S. Cong, "Second-order sliding-mode-based synchronization control of cable-driven parallel robots," *IEEE/ASME Trans Mechatron* **25**(1), 383–394 (2020).
[26] Q. Qin and G. Gao, "Screw dynamic modeling and novel composite error-based second-order sliding mode dynamic control for a bilaterally symmetrical hybrid robot," *Robotica* **39**(7), 1264–1280 (2021).
[27] M. Barghandan, A. A. Pirmohamadi, S. Mobayen and A. Fekih, "Optimal adaptive barrier-function super-twisting nonlinear global sliding mode scheme for trajectory tracking of parallel robots," *Heliyon* **9**(2), e13378 (2023).
[28] C. Schenk, C. Masone, A. Pott and H. H. Bülthoff, "Application of a differentiator based adaptive super-twisting controller for a redundant cable-driven parallel robot," *Mech Mach Sci* **53**, 254–267 (2017).
[29] S. P. Bhat and D. S. Bernstein, "Finite-time stability of continuous autonomous systems," *SIAM J Control Optim* **38**(3), 751–766 (2000).
[30] M. A. Sepestanaki, A. Jalilvand, S. Mobayen and C. Zhang, "Design of adaptive continuous barrier function finite time stabilizer for TLP systems in floating offshore wind turbines," *Ocean Eng* **262**(15), 1–21 (2022).
[31] A. Polyakov, "Nonlinear feedback design for fixed-time stabilization of linear control systems," *IEEE Trans Automat Control* **57**(8), 2106–2110 (2012).
[32] R. Xu, D. Tian and Z. Wang, "Adaptive disturbance observer-based local fixed-time sliding mode control with an improved approach law for motion tracking of piezo-driven microscanning system," *IEEE Trans Ind Electron* **71**(10), 1–14 (2024).
[33] B. Wang, H. Jahanshahi, C. Volos, S. Bekiros, A. Yusuf, P. Agarwal and A. A. Aly, "Control of a symmetric chaotic supply chain system using a new fixed-time super-twisting sliding mode technique subject to control input limitations," *Symmetry* **13**(7), 1257 (2021).
[34] Z. Zuo, Q. Han, B. Ning, X. Ge and X. Zhang, "An overview of recent advances in fixed-time cooperative control of multiagent systems," *IEEE Trans Ind Inf* **14**(6), 2322–2234 (2018).
[35] D. Ba, Y. X. Li and S. Tong, "Fixed-time adaptive neural tracking control for a class of uncertain nonstrict nonlinear systems," *Neurocomputing* **363**, 273–280 (2019).
[36] E. A. Barbashin, "Introduction to the theory of stability," (1967).
[37] V. I. Utkin, "Sliding modes and their application in discontinuous systems," *Automat Remote Contr* **21**, 1898–1907 (1974).
[38] D. S. Broomhead and D. Lowe, "Radial basis functions, multi-variable functional interpolation and adaptive networks," (1988).

Cite this article: X. Li and G. Gao (2024). "An intelligent fixed-time super-twisting sliding mode control of the uncertain hybrid mechanism", Robotica **42**, 3532–3551. https://doi.org/10.1017/S0263574724001516